JOURNAL OF GEOPHYSICAL RESEARCH, VOL. 112, C03003, doi:10.1029/2006JC003924, 2007

Surface current effects on the fetch-limited growth of wave energy

Brian K. Haus[1]

Received 5 September 2006; revised 20 October 2006; accepted 30 October 2006; published 6 March 2007.

[1] To study the fetch-limited growth of wind wave energy over a region with significant lateral shear of the current field, this study exploited data obtained from two linear phased-array High Frequency (HF) radar systems. Both the near-surface currents and wave energy and period were mapped over the highly sheared inshore boundary of the Florida Current. The wave energy growth during two periods when the winds were steady for >12 hours and were directed offshore was computed over a range of fetches from 5 to 45 km. The observed energy growth rates were significantly (~50 %) lower than predicted by the Donelan et al. (1992) empirical formulation over the high vorticity region. The reduced growth rate was consistent with a shift of the wind stress direction into the current direction due to refraction of the wave field. Dimensionless wave energy increased by as much as 100% over neighboring values when the vertical component of the surface current vorticity was a global minimum. While trapping and enhancement of wave energy is predicted by wave ray theory, it has never before been confirmed within the Florida Current with coincident wave and current measurements.

Citation: Haus, B. K. (2007), Surface current effects on the fetch-limited growth of wave energy, *J. Geophys. Res.*, *112*, C03003, doi:10.1029/2006JC003924.

1. Background

1.1. Fetch-Limited Wave Growth

[2] For effective wave modeling it is necessary to specify the transfer of energy or action from surface winds to surface waves. While the wind input term is of fundamental importance to wave modeling, its accurate estimation has been elusive primarily because of the difficulty of making precise measurements in the field. Wave energy growth with increasing fetch when the wind is directed offshore provides the most tractable situation for study. However even this special case, field observations of fetch-limited wave growth are complicated by a number of factors that have led to significant variability in the results.

[3] Early efforts to define a universal growth curve relating a characteristic wind velocity (usually U_{10}, the wind referenced to a height of 10 m above the surface) included the JONSWAP [*Hasselmann et al.*, 1973] curve and the SMB [*CERC*, 1977] curves both of which defined a power law growth rate. Experiments by *Donelan et al.* [1992] showed that the power law did not correctly represent the wave growth at longer fetches. They presented differential empirical growth curves that related the dimensionless fetch ($\tilde{X}$) to the dimensionless energy ($\tilde{E}$) following the scaling proposed by *Kitaigorodskii* [1962]. A fundamental question posed by their work was whether it was appropriate to expect that a universal growth curve was anything other than a theoretical abstraction, given the large number of complicating factors. Among these factors were the temporal and spatial variability of the wind field, local topography in shallow water [*Young*, 1997], the difficulty in determining the fetch over which the waves have been forced [*Dobson et al.*, 1989], the presence of swell and stability effects. Recent re-analysis of multiple existing data sets by *Hwang* [2006] reconciled some of the discrepancies by scaling the reference wind by $U_{\lambda/2}$ instead of U_{10} as suggested by *Donelan* [1990]. Where $U_{\lambda/2}$ is the more physically relevant wind velocity at a height of $^1/_2$ the ocean wavelength.

[4] The effects of surface currents and surface current shears have not been included in most of these analyses, although it is clear that there can be a significant effect of currents on wave energy propagation [*Kudryavtsev et al.*, 1995; *Shay et al.*, 1996; *Walsh et al.*, 1996; *Haus et al.*, 2006]. Globally there are several continental shelf regimes where strong mean currents contribute significantly to the shelf dynamics. In this broader context, there is a lack of concurrent measurements of wind-waves and currents with sufficient spatial and temporal sampling resolution to resolve wave-current interaction issues.

1.1.1. Effects of Uniform Currents

[5] For uniform currents there are two primary effects on wave propagation, which have typically been divided into effects on wave kinematics and dynamics [*Jonsson*, 1990]. Additionally, the wind moving over a surface in motion will have a higher relative velocity for currents moving into the wind and a lower relative velocity when the wind and currents are aligned. This has a direct impact on the fetch-limited wave growth rate. It can accounted for in the *Donelan et al.* [1992] curve and other treatments by adjust-

[1]Division of Applied Marine Physics, Rosenstiel School of Marine and Atmospheric Science, University of Miami, Miami, Florida, USA.

0148-0227/07/2006JC003924$09.00

ing the observed wind speed for this shift in relative motion using,

$$\left(\mathrm{Ur} = \mathrm{U}_{10} - U_a^0\right), \tag{1}$$

where U_a^0 is the alongwind component of the surface current velocity and U_{10} is the wind speed at 10-m above the water.

[6] The kinematic effects for developing waves include effects on the wave phase velocity ($\mathrm{C_p}$) and the wavenumber (k). The absolute phase velocity for waves moving over uniform currents will be shifted away from the relative phase speed (C_r) by the current component in the wave direction (U_w^0) such that,

$$C_p = C_r + U_w^0, \tag{2}$$

The wavelength of the wave will be proportionally shortened (lengthened) in an opposing (following) current.

[7] The dynamic effect on the surface waves that are moving over the current field can be derived from energy or action conservation equations. Wave heights will increase (decrease) when waves are moving against an opposing (following) current. The strength of this effect depends on the incident wavenumber and direction relative to the current direction and magnitude. The high wavenumber portion of the gravity wave spectrum is most strongly impacted by currents because it has lower group velocities. The forward propagation of short gravity waves ($\mathrm{k} > 6$) will be completely halted by currents greater than 1 ms^{-1}. The critical opposing current velocity (U_c^0) for a particular k is given by,

$$U_c^0 = \frac{C_g'}{2}, \tag{3}$$

where C_g' is the deepwater incident wave group velocity [*Mei*, 1989]. For fully developed seas under moderate winds much of the wave energy will be at wavenumbers such that the group velocity will not approach U_c^0 for currents less than 1.5 m s^{-1} [*Haus et al.*, 2006]. Under light winds, young seas or fetch-limited conditions a significant proportion of the wave energy resides at high wavenumbers where unbounded growth will occur in regimes with weaker opposing currents.

1.1.2. Horizontally Sheared Currents

[8] Traditionally it has been assumed that any effect of horizontally sheared currents on wave development will be transmitted only through the effect that the currents have on the local wave field, neglecting effects on the coupling between the wind and the waves. Because the speed of wave propagation changes as waves move across variable currents or topography the direction of propagation of the waves will also change. There has been a long history of research on waves propagating through current fields, with most of the effort focused on monochromatic, linear waves that are not under the direct influence of wind-forcing.

[9] For waves propagating obliquely into a sheared current their ray-paths will be curved. *Kenyon* [1971] demonstrated that in cases of weakly sheared flow and weak current magnitude (U^0) relative to the wave group velocity (Cg), such that $\mathrm{U}^0/\mathrm{Cg} \ll 1$ the ray curvature (ψ) is approximately equal to the ratio between Cg and the vertical component of surface current vorticity (υ)

$$\psi = \frac{C_g}{\upsilon} \tag{4}$$

where $\upsilon = \left(\frac{\partial U_y^0}{\partial x} - \frac{\partial U_x^0}{\partial y}\right)$. This result has several important implications. First, for a given current field the radius of curvature increases in proportion to the group velocity. Furthermore following (opposing) waves traveling over a sheared current will be refracted in the direction of decreasing (increasing) current speed. This then allows conditions under which following (opposing) waves can be trapped in a local minimum (maximum) of current speed, forming regions of caustics and shadow zones as observed by *Shay et al.* [1996] for waves propagating over a warm core ring of the Gulf Stream.

[10] *MacIver et al.* [2006] measured wave refraction on both horizontally and vertically sheared currents in the laboratory. Their results confirmed the basic structure predicted by ray theory based on the mild shear assumption. They observed opposing waves bending toward the current normal and increasing in height and following waves bending toward current parallel and decreasing. Application of a moderate shear model which was more appropriate to the conditions in the laboratory did not significantly improve comparisons with observed wave refraction.

[11] The inverse problem of inferring current velocities from changes in wave propagation has been investigated from satellite observations [*Beal et al.*, 1997; *Cornillion and Park*, 2001]. Based on concurrent upper ocean current profiles and directional surface wave measurements from a scanning radar altimeter, *Shay et al.* [1996] and *Walsh et al.* [1996] observed that low frequency surface waves were significantly affected by the near-surface current vorticity field in a Gulf Stream warm core ring. A simple ray tracing model indicated that the swell portion of the wave field ($\sim$10 sec waves) was refracted to form a caustic region 80 to100 km to the east of the warm core ring. By contrast, weaker caustic regions were found along the west side of the oceanic feature. These studies concluded that the surface current structures need to be resolved to understand the interactions between the wave and current fields.

[12] Direct observations of the effect of sheared currents on developing waves have been limited. *Kudryavtsev et al.* [1995] observed the refraction and reflection of wind waves from the Gulf Stream frontal edge using marine radars during ship crossings. They suggested that wave refraction over sheared currents could be responsible for changes in wave growth rates, however they were not able to quantify this effect because the marine radars did not provide absolute wave energy measurements. Regions of trapped waves when the winds were in opposition to the current direction led to large vertical displacements of the research vessel.

[13] In most treatments of wind stress on the ocean surface the magnitude of the stress is estimated from the wind speed at some level above the surface by the use of the bulk momentum transfer coefficient $\mathrm{C_D}$. The stress direction is typically assumed to be in the wind direction, although measurements have shown that this is often incorrect. For

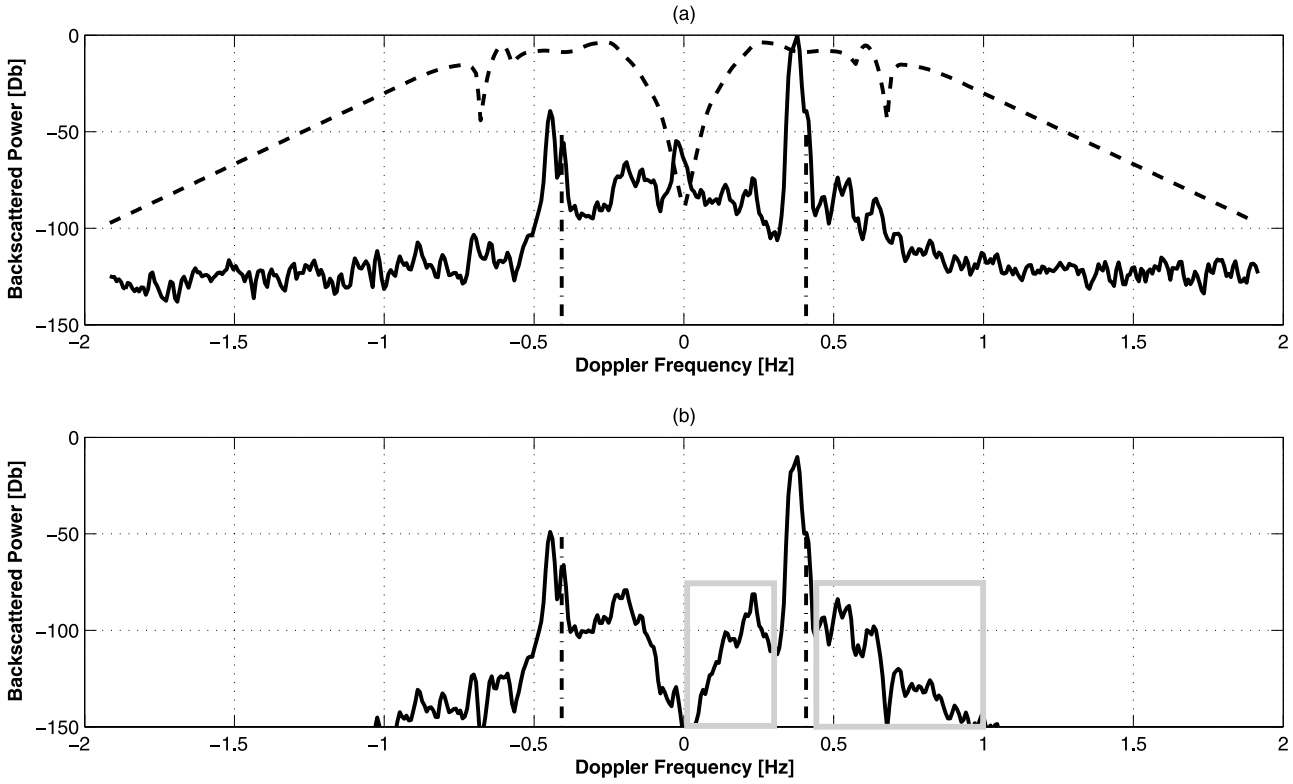

Figure 1. (a) Typical echo-Doppler spectrum (solid line) as observed by WERA as deployed off SE Florida. Db scale normalized by peak of backscattered spectrum. Bragg peaks for 16.045 MHz are shown with dash-dotted line. Weighting function as derived by *Barrick* [1977] shown with dashed line. (b). Spectrum normalized by weighting function. Second-order regions used for wave heights shown in gray boxes with the boundary closest to the first-order peak determined by the location of the spectral null. Only values in more energetic half space were used in wave calculations.

example, *Zemba and Friehe* [1987] observed large angles between the wind and the wind-stress vectors in aircraft measurements over the California current. *Geernaert* [1988] observed a significant deviation of the wind-stress from the wind direction in tower studies in the North Sea. The orientation of the deviation depended upon the local stability, in stable conditions the wind stress was rotated to the left of the wind vector while in unstable conditions it was rotated to the right. It has also been observed by *Geernaert et al.* [1993], *Rieder et al.* [1994] and *Grachev et al.* [2003] that swell waves can induce deviations in the stress direction.

[14] Recent measurements of wind stress and waves using buoys and HF radar observed surface currents by *Drennan and Shay* [2006] have shown that surface currents can cause the wind stress direction to shift away from the wind direction. They inferred that this wind stress shift resulted from the refraction of the peak waves toward the current direction. This then caused the short waves that support most of the stress to be shifted as well.

[15] The objective of this study was to determine if horizontally sheared currents reduced the fetch-limited growth rate of surface waves as expected if the wind stress vector was steered away from the wind vector. Surface wave energies and near-surface currents were simultaneously observed using HF Radars. The radar measurements and the technique used to extract the wave energies from the radar echo-Doppler spectrum is described in section 2. Two case studies were analyzed when the wind was steady and directed offshore for a period of at least 12 hours (section 3). The region over which the waves were developing included the Florida Current (FC) and consequently the waves were significantly affected by the strong mean currents and horizontal current-shear. The effect of the currents on the fetch-limited wave growth and on trapping of wave energy was explored. This is followed by a summary of the results in section 4.

2. Methods

2.1. HF Radar Wave Measurements

[16] In addition to the 1st order Bragg resonances first observed by *Crombie* [1955] a typical HF radar derived echo-Doppler spectra contains significant energy at frequencies around the 1st order peaks (Figure 1). These second-order returns contain backscattered energy resulting from multiple reflections of the radar signal as well as the hydrodynamic combination of surface waves to produce a Bragg scattering wave [*Barrick*, 1977]. The second-order portion of the Doppler spectrum therefore contains information on the surface waves.

[17] Methods to invert the 2nd order contribution to the Doppler spectrum to estimate the surface wave directional spectrum have been developed by *Wyatt* [1990] and *Howell*

and Walsh [1993]. These methods require that the observations from two overlapping radar stations be available, as in the case for current vector retrievals. However, because the second order returns have a lower signal to noise ratio (SNR) than the 1st order returns their use is usually limited to about 50% of the range over which current measurements are obtained. This makes the overlapping requirement much more restrictive than for current observations [*Wyatt et al.*, 2005]. *Wyatt et al.* [1999] demonstrated that such dual-site inversion methods can obtain reliable wave spectral estimates when compared with moored buoys. *Hisaki* [2005] has produced wave spectral estimates using a blend of single site radar observations and a wave model. This hybrid approach is likely to be quite useful for extending the range of HF wave observations, but is of limited use for focused wave studies because the wave field has been assumed to take a specified form.

[18] Historically, for field operations the large amount of disk storage required to archive the raw data was often difficult to manage. The large data storage capacities required is no longer a significant limiting factor, however transmission bandwidth from remote sites can limit near real-time wave directional spectra observations. Single site Doppler spectra can be processed on site to obtain and transmit wave parameters such as the significant wave height (H_s) and mean period (T_m) using the scaled ratio between the 2nd order and 1st order returns [*Barrick*, 1977; *Heron et al.*, 1985]. Single site extraction of wave parameters also can be used to expand the range of coverage outside the region of overlap between two sites.

[19] Direction-finding HF radars can only collect echo-Doppler spectra for given ranges integrated over large azimuths. In practice this limits the scientific use of the direction-finding wave observation because it requires that the coastal wave field be homogeneous over large spatial domains. Additionally the 1st order Bragg peaks are significantly spread by the range of observed current velocities so that there is limited access to the second order structure. In contrast the use of beam-forming techniques with a linear phased-array receiver provides the echo-Doppler spectrum at every range and azimuth bin.

[20] Empirically based methods have been tested and validated for the phased-array Ocean Surface Current Radar (OSCR) HF radars by *Graber and Heron* [1997]. Their approach was extended and extensively tested by *Ramos* [2006], where rms differences of Hs between 0.21–0.50 m were found in comparisons with multiple in situ observations. Although larger differences were expected in regions of high spatial variability of the wave field because of the spatial smoothing inherent in the radar observations, the observed differences were of the same order as those typically found between in situ observations [*Graber et al.*, 2000]. The empirical method was used to observe the interaction of incoming surface waves with the Chesapeake Bay outflow plume by *Haus et al.* [2006]. Increased Hs associated with an opposing current on the outgoing tide was successfully localized in both space and time, thereby demonstrating the utility of the approach for making spatially distributed wave height measurements.

[21] The empirical method of *Ramos* [2006] uses the ratio between the second order peaks (Figure 1), scaled by a weighting function [*Barrick*, 1977] to define the directionally integrated wave parameters H_{rms} (5) and the mean period T_m (6).

$$H_{rms}^2 = \frac{2\alpha^2}{k_o^2} \frac{\int_{-\infty}^{\infty} [\sigma_{(2)}(f_d) W(f_d)]\, df_d}{\int_{-\infty}^{\infty} \sigma_{(1)}(f_d)\, df_d} \tag{5}$$

$$T_m = \frac{\beta}{f_B} \frac{\int_{0,f_B}^{f_B,\infty} \sigma_2(f_d) W(f_d)\, df_d}{\int_{0,f_B}^{f_B,\infty} \left| f_d/f_B - 1 \right| [\sigma_2(f_d) W(f_d)]\, df_d} \tag{6}$$

where σ_1, σ_2 are the first and second order backscattering cross-sections, f_d is the Doppler frequency, f_B is the Bragg wave frequency and k_0 is the radar wavenumber. $W(f_d)$ is a weighting function that is used to suppress the zero-Doppler returns and energy far removed from the Bragg peaks. The parameters α, β are empirically determined constants. The shape of $W(f_d)$ is shown along with an example spectrum in Figure 1a. After multiplying by $W(f_d)$ the remaining energy (Figure 1b) is integrated over the half of the spectrum that contains the most energy in the 1st order peak. The limits in (6) indicate that the integration can be performed from $0 \leq f_d \leq f_B$ or $f_B \leq f_d \leq \infty$, the choice of which limits to use depends on the Doppler spectrum characteristics. In practice narrower bounds are used that begin from the null of the 1st order Bragg peaks (Figure 1b).

2.2. Wellen HF Radar System

[22] The HF radars used for these studies were a pair of Wellen Radars (WERA) which are phased-array systems that use frequency modulated continuous wave transmission (FMCW) to interrogate the ocean surface. WERA performance was first demonstrated for surface current mapping by *Gurgel et al.* [1999]. *Essen et al.* [2000] compared WERA observations to a bottom mounted S4 current meter and found better agreement between the WERA and the S4 than a CODAR HF radar and the same current meter. *Shay et al.* [2007] provided extensive validation of the surface current measurements with ADCPs on the west Florida shelf. They found excellent agreement between the WERA observations and near-surface bins of ADCPs. The rms differences along radar radials were less than 0.06 ms^{-1} and the linear correlation coefficients ranged from 0.81 to 0.94.

2.3. HF Radar Measurements Over the SE Florida Shelf

[23] A pair of WERA HF radars were deployed in June 2004 as a component of the Southeast Atlantic Coastal Ocean Observing System (SEACOOS) to observe surface currents and waves over the SE Florida shelf (Figure 2). WERA as deployed in SEACOOS consists of two transmit/receive stations each with a linear 16-element phased-array receiver and a rectangular 4-element transmitter (Table 1). The system is operated at 16.045 MHz which scatters off a Bragg ocean wavelength of 9.35-m.

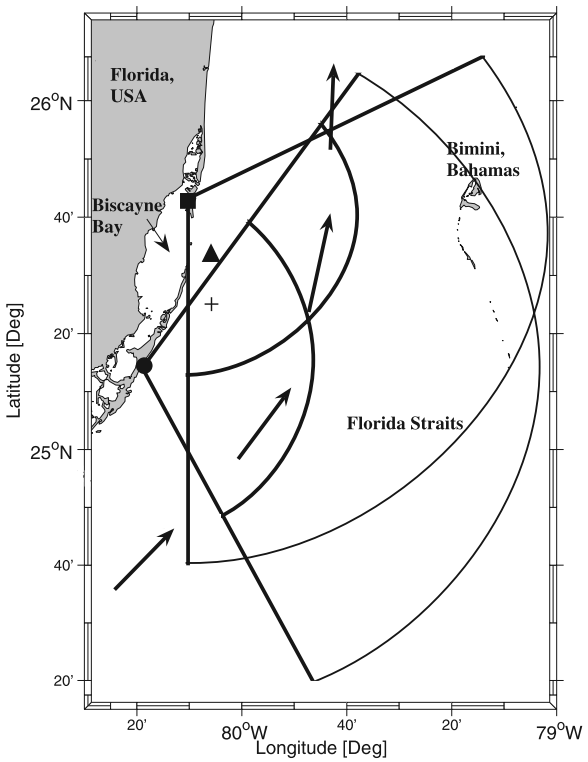

Figure 2. Coverage area of WERA stations as deployed for SEACOOS. Outer semicircle is the radial coverage from each station. Inner semicircle is the typical wave measurement limit from each station. Solid black square denotes the location of the Key Biscayne WERA site. Solid black circle is the Key Largo WERA site. Triangle denotes location of FWYF1 used for wind and air-sea temperature measurements. Cross marks the location of the Sontek ADP and Triaxys buoy used for wave measurement calibration and validation. Arrows show the general flow direction of the Florida Current.

[24] Because of limited accessible coastline the two radar stations were positioned at a distance of ~50-km from each other. This provided a large area for current mapping, with the region of consistent current vector retrievals extending well out over the Florida Straits (Figure 2). The large distance between stations limited the region for which directional spectra could be measured using two-site methods to a relatively small area [*Wyatt et al.*, 2005]. However, because the empirical approach does not require overlap between two stations, a large area was available over which wave parameters were observed.

[25] *Ramos* [2006] studied the consistency of the parameters α and β (5, 6) and found that α was quite robust and didn't need to be adjusted to fit observed OSCR data over a period of 5 years and multiple experiments. Although β also did not change significantly, there was higher variance in the period measurements than for wave height. These values were used as initial guesses for the WERA wave observations, but were modified after calibration and validation studies conducted in spring 2005. H_{rms} and T_m derived from (5, 6) were compared to H_s and T_m observed with a Sontek wave observing Acoustic Doppler Profiler (ADP) over a 25 day period (Figure 2). The parameters (α and β) that provided the best fit to the in situ H_s and T_m were then used to scale the radar H_{rms} and T_m.

Table 1. WERA System Characteristics as Deployed Over the Southeast Florida Shelf

Operating frequency	16.045 MHz
Transmitted peak power	30 W
Bragg wavelength	9.35 m
Nominal measurement depth	0.8 m
Operational range	80–120 km
Range cell resolution	1.2 km
Integration time	5 min
Samples per measurement	1028 samples
Azimuthal resolution	2°
Radial component accuracy	2 cm s^{-1}
Sample repeat period	20 min

[26] The calibrated WERA observed H_s and T_m were compared with a different 45-day series of Tri-axys directional wave buoy observations. The rms differences between the Key Biscayne radar observed H_s and T_m and the buoy H_m0 and T_m extracted from the observed wave spectra were 0.20 m and 0.71 s respectively. The variability of the WERA observed parameters was consistent with that observed in multiple HF-radar comparisons with in situ observations by *Ramos* [2006]. Although the H_s, T_m measurements from the Key Biscayne radar station had significant scatter, means over 6-12 hour periods were of sufficient accuracy (Table 2) to proceed with the analysis of wave energy growth.

3. Case Studies of Fetch-Limited Growth Over Sheared Currents

[27] For the purposes of this study it was important to isolate the effects of surface currents from other influences on wave growth. The Florida Straits is an almost ideal area in which to study the effects of strong currents and current shear on wave growth, because of the presence of the Florida Current. The region is also rarely exposed to nonlocally generated swell waves which are dissipated over the shallow banks of the islands of the Bahamas lying ~100-km to the east. Complicating factors that could be important to consider here are the transition from the land-air boundary layer to the sea-air boundary layer, temporal variability of wind speed and direction, depth-limited waves and stability effects.

3.1. Study Region

[28] The coastline of SE Florida is gently curving with generally quasi-linear local shorelines, the exception being the opening into Biscayne Bay (Figure 2). Although there

Table 2. Average (Over Fetch) of Mean Values and 95% Confidence Intervals Based on Sample Variances and t-Distributions for Significant Wave Height (Hs), Mean Period (T_m) and the Alongwind Component of the Surface Current (U_a^0) From WERA Observations and the Neutral 10-m Equivalent Wind Speed (U_{10N}) From the NOAA Fowey Rocks CMAN Station (FWYF1)

	Hs, m	T_m, s	U_a^0, m s^{-1}	U_{10N}, m s^{-1}
YD 356	0.68 ± 0.06	4.55 ± 0.16	−0.51 ± 0.03	10.47 ± 0.038
YD 361	0.43 ± 0.06	4.36 ± 0.27	−0.80 ± 0.04	8.58 ± 0.025

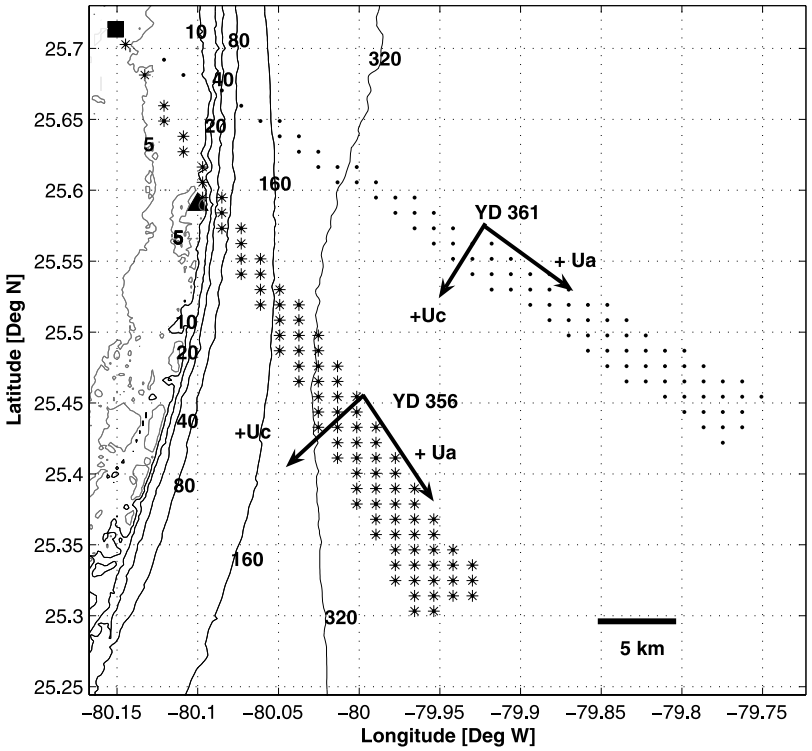

Figure 3. Topography of measurement area in meters. Solid black square denotes positon of Key Biscayne WERA site. Solid triangle marks the location of FWYFI. WERA cells used for study on YD 356 are shown with asterisks, and for YD 361 with dots and axes rotated in wind direction are displayed in each case. Each sector of cells for the two days is proscribed by those locations lying within 3 degrees of the mean wind direction and a total distance from the radar of less than 50 km.

are only small islands along the offshore edge of Biscayne Bay, between the islands the depths are very shallow. Rock banks are often exposed at low-tide although the tidal range is typically less than 0.7-m. The shallow banks are only cut by narrow curving channels, therefore the apparent gap is actually an effective barrier to wave propagation. This makes relatively simple to define the local fetch in the study region when the wind is blowing offshore.

[29] The natural surface topography in SE Florida is quite flat with maximum relief of only a few meters and vegetation that is generally short due to adaptation to tropical storms. However in developed areas there are many large multi-story buildings located close (within 100-m) of the shoreline. The wind blowing over these towers may require significant fetch to reestablish an unperturbed boundary layer flow [*Donelan et al.*, 1992]. One of the advantages of the radar measurements is that many different fetches can be observed and the extent of the effect of disturbances to the boundary layer can be assessed.

[30] The typical range over which reliable wave observations were extracted from the WERA systems was from 5-km to 40-km. This allowed measurements extending from the shallow shelf (depths < 10-m) offshore of Key Biscayne, Florida well out into the Florida Straits (Figure 3). The distance from the Key Biscayne radar station to the outer fringing reef edge (defined where the depth reached 10-m) in the wind direction was 10-km on YD 356 and 7-km on YD 361. Offshore of the fringing reef the shelf drops off sharply to depths over 100-m within 3-km.

[31] The tidal velocities over the inner-shelf are typically weak, except near inlets and channels [*Fiechter et al.*, 2006]. The shelf currents are primarily wind-driven, particularly in the winter months when frontal passages provide stronger forcing [*Haus et al.*, 2000]. The typical current velocities offshore of the inner-shelf are strongly affected by presence of the Florida Current (FC) which is constrained to flow through the Florida Straits. Typical current velocities within the FC exceed 1.5 m s^{-1} although there is significant variability on scales ranging from weekly to yearly [*Mooers and Fiechter*, 2005]. There are high lateral shear zones along both edges of the FC; however, the strongest shears typically are observed along the western boundary. In this region the Rossby number, defined by

$$(Ro = \nu / f_C)$$

where f_C is the local Coriolis parameter, often exceeds 1 [*Winkel et al.*, 2002] in the upper 100-m. The western edge of the FC, usually lies within 20-km of the shelf break [*Haus et al.*, 2000], which is well within the range of the WERA wave and current observations. There is significant variability in the position of this western wall, and the FC is perturbed by frontal eddies of many scales from a few km [*Shay et al.*, 2000] to over 70-km [*Haus et al.*, 2004].

3.2. Wind Forcing

[32] The wind velocity and air and water temperatures throughout the experiment were available at the Fowey

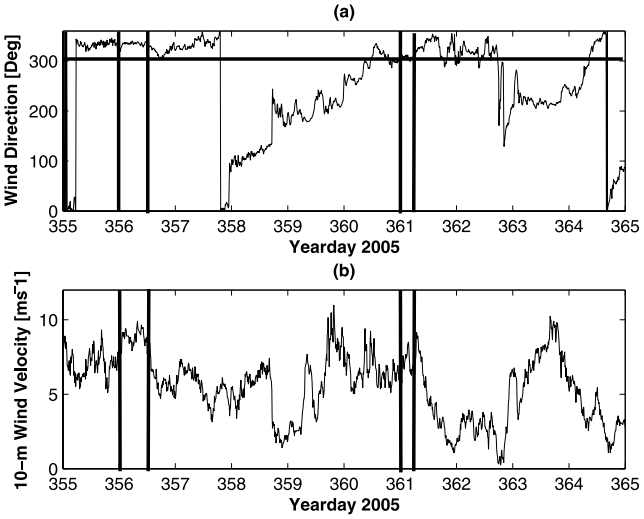

Figure 4. FWYF1 CMAN station observed winds at height of 43.9 m during December 2005 converted to 10-m neutral values. The two periods of interest are marked with solid vertical bars. (a) Wind direction (from) in degrees from true North. Solid horizontal line marks the look direction of the Key Biscayne radar. (b) Wind speed (m s^{-1}).

Rocks NOAA CMAN (FWYF1) station (Figure 4). The station is on a tower mounted in ~3-m of water along the outer edge of the reef tract. The anemometer at FWYF1 was 43.9-m above the mean water level (MWL). The air temperature was recorded 11-m above MWL and the water temperature was recorded 1 m below the MWL.

[33] During the wintertime in SE Florida offshore winds often lead to an unstable air-sea regime, the air-sea temperature difference at the tower was ~10°C on both YD 356 and 361 (Figure 5). A neutrally stable log-profile was used to convert the observed wind speed to an equivalent neutral 10-m wind speed, with the coefficients chosen as in *Drennan and Shay* [2006]. Here the local air and sea temperatures and the wind were used in an iterative calculation ignoring the effects of stability in the first step. A limitation of the study is that there was only one in situ temperature measurement made with fetch. Therefore we could not directly evaluate how much the stability may have changed over the FC. However from AVHRR imagery (Figure 6) it can be seen that the FC was 2°C warmer than the inner shelf water, therefore the air-sea interface remained unstable.

[34] A 10 day span in late December 2005 was selected for further study because the storm fronts in late fall in south Florida often produce offshore winds. The full 2 year record is available in archives for further processing as desired, however for the purposes of providing case studies the short period chosen was sufficient. Inspection of the wind record revealed two periods when the wind was relatively steady and offshore for at least 12 hours (Figure 4).

[35] The wind direction (to) during these two relatively steady periods was 155° and 128°, respectively. This placed the wind direction within 32° of the boresight (orthogonal to receive array) of the Key Biscayne radar (122°) for YD 356 and 6 ° for YD 361. For North Key Largo the wind direction was at larger angle (64°, 38°) to the radar receiver boresight (91°). The Key Biscayne station could then observe the wave energy in the wind direction with all the measurements located close to the boresight. This minimized any potential effects of antenna beam side lobe contamination on the wave observations [*Haus et al.*, 2004], and made the Key Biscayne station the appropriate choice to study the fetch-limited growth in each case.

3.3. Surface Currents

[36] The near-surface current velocity could not be measured using the combination of both radar site radials at all locations for each wind direction. This is because the angle between radials must be >30° to keep the errors when combining to produce vectors within reasonable limits [*Graber et al.*, 1997]. For this study this caused the shortest fetches to be unavailable for vector current observations. The initial fetch where the currents were available for YD 356 and YD 361 was 15-km and 17-km respectively. The vector currents were rotated into a coordinate system aligned with the wind direction (Figure 7) for each period of interest. The alongwind (U_a^0) and cross-wind (U_c^0) surface current components were then extracted with positive alongwind currents being in the wind direction and positive cross-wind currents being directed to the right of the wind vector.

[37] The currents were relatively weak (for the FC) on YD 356 and were generally aligned in opposition to the wind (Figure 7a). The ratio of current velocity to the wave group velocity was less than 0.2 until 35-km offshore. At short fetch on YD 356 the current was in the wind direction, but then as the FC influence increased the current switched to opposing the wind direction. The crosswind component on YD 356 ranged from -0.25 ms^{-1} to a maximum negative velocity of -0.5 m s^{-1} far offshore. Out to 25-km offshore the alongwind shear of the crosswind velocity was positive, then it was close to zero for 10-km when it

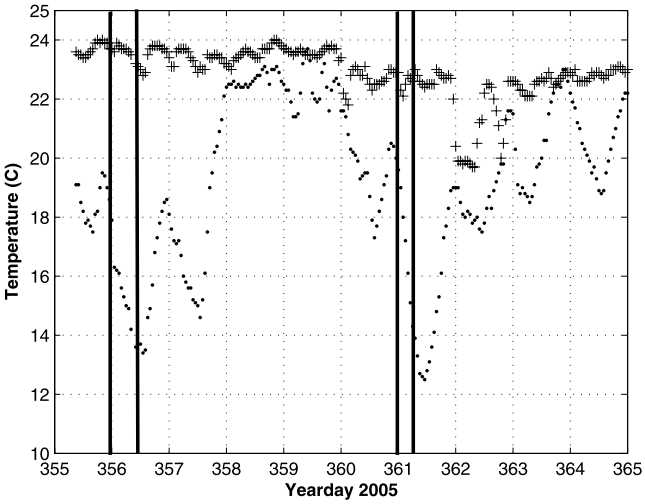

Figure 5. Air (dots) and water (pluses) temperatures recorded at FWYF1 during period of interest. Air temperature recorded at 11 m, water temperature at 1 m depth. Times of case studies shown by vertical bars.

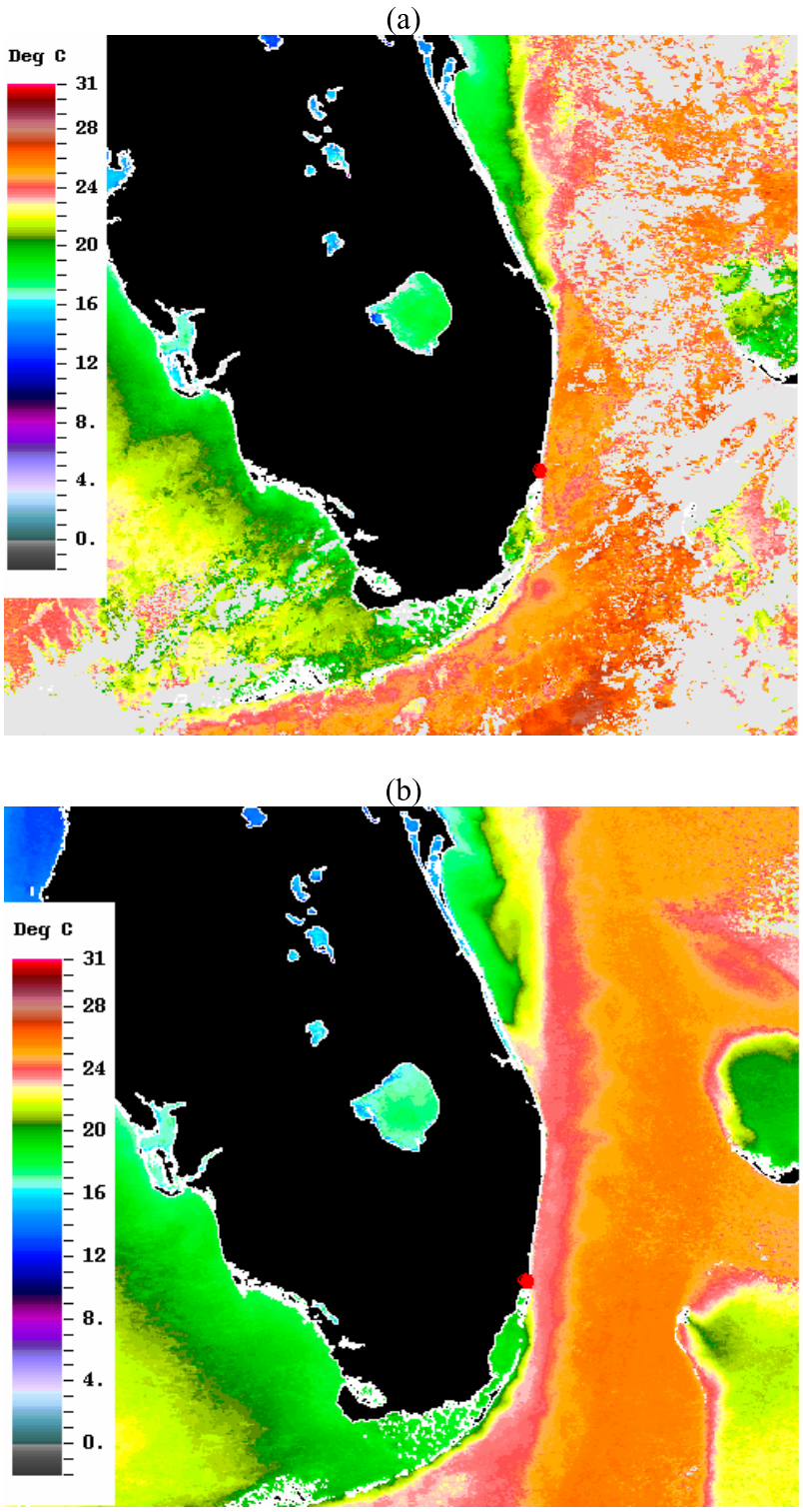

Figure 6. Daily composite of AVHRR derived SST processed by the Institute for Marine Remote Sensing (IMaRS) at the College of Marine Sciences, University of South Florida. Colorbar shown at left. Key Biscayne WERA site marked with a red circle. (a) YD 356 and (b) YD 361.

became increasingly negative with fetch. On YD 361 U_a^0 was consistently in opposition to the wind, while U_c^0 was larger, reaching 1.5 ms^{-1} (Figure 7b). The alongwind shear of U_c^0 was large and negative until 20-km offshore.

3.4. Fetch-Limited Wave Growth

[38] H_s and T_m as defined in (4, 5) over sectors within 3° of the wind direction and within 50-km of the transmitter/receiver (Figure 3) were extracted from the Key Biscayne radar echo-Doppler spectra for each case. These bounds

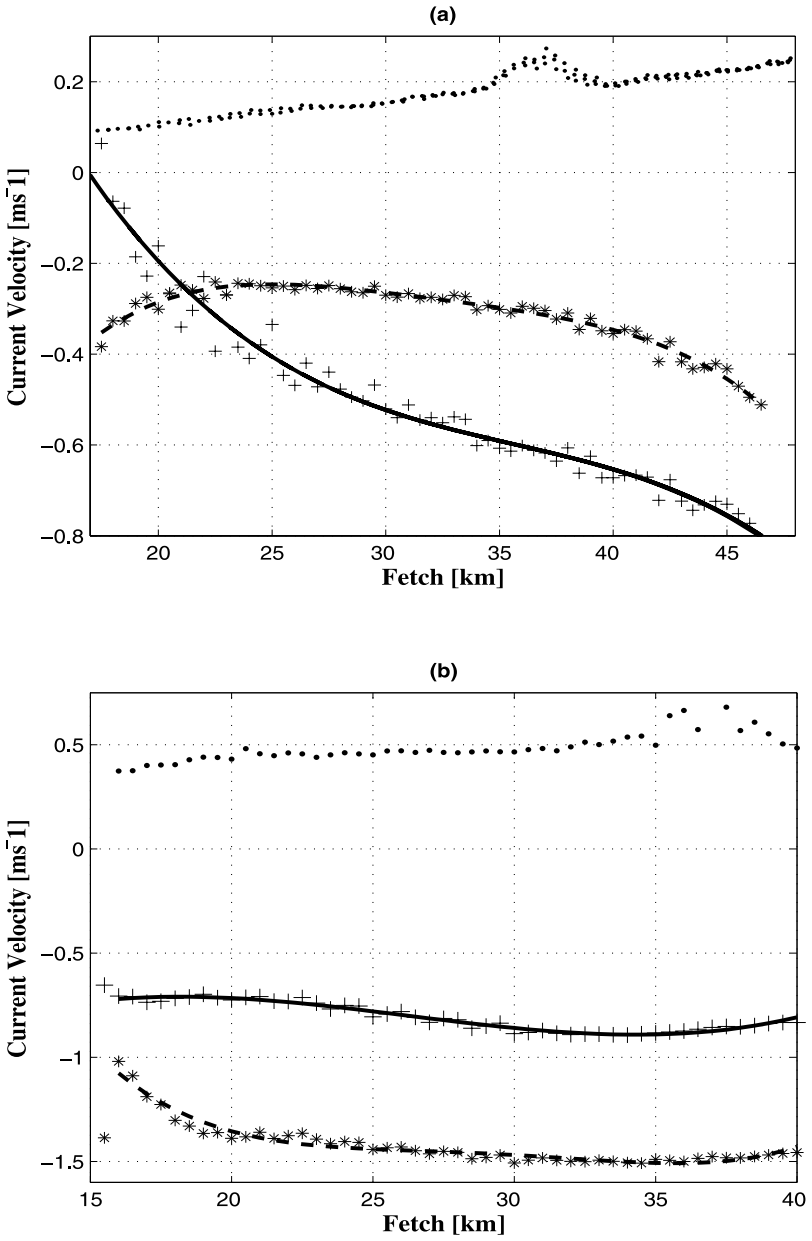

Figure 7. Averaged horizontal near-surface currents for period of wave observations alongwind currents (U_a^0) with positive currents in the wind direction (pluses). Cross-wind currents (U_c^0) positive when directed to the right of the wind vector (asterisks). Current magnitude scaled by the wave group velocity (ψ) (dots). (a) YD 356 and (b) YD 361.

were based on the 3-Db down point of the radar receiver beam pattern and the nominal limit of 50% of the range for which the currents could be observed. The 20-minute sample values were averaged for the first 12 hours of YD 356 (36 observations) and for the first 6 hours of YD 361 (18 observations). No spatial smoothing or averaging was done on either the H_s or T_m measurements.

[39] The observed rms differences for H_s, T_m between the Key Biscayne radar and the Tri-axys buoy derived from the validation studies (0.20-m, 0.71-s) provided bounds on the errors. By attributing all of the differences to radar error in each case the standard error of the mean (χ) can be defined by $\chi = \sqrt{\sigma^2/N}$, with N = number of observations and σ^2 = variance (or mean square error in this case). The standard error of H_s and T_m were then bound by ±0.06 m and ±0.12 s on YD 356 and ±0.08 m and ±0.17 s on YD 361.

[40] Alternatively, the variance of the 20 minute samples that were averaged to produce the mean wave energy was used to calculate the standard error of the mean at each location. On YD 356 the standard error of H_s (T_m) ranged from 0.01 m (0.04 s) close to the shoreline to 0.05 m (0.12 s) offshore. On YD 361 the standard error of H_s (T_m) had roughly the same range 0.006 m (0.07 s) close to shore with a maximum of 0.06 (0.37 s), even though the number of samples was smaller. These values were within the bounds determined from comparisons with the in situ observations, except for the wave period on YD 361. No running average filter was employed on T_m in this case,

which could explain the higher errors. The 95% confidence intervals on the observed quantities were then computed using the t-distribution and the respective sample sizes for the two case studies (Table 2).

[41] Exploiting linear wave theory and the radar measurements of H_s and T_m, the total wave energy and group velocity were estimated using the standard formulation ($E = \frac{H_S^2}{16}$, $C_g = \frac{gT_m}{4\pi}$). The nondimensional fetch ($\tilde{X}$) and energy ($\tilde{E}$) were expressed using the *Kitaigorodskii* [1962] scaling such that $\tilde{X} = \frac{Xg}{U_{10N^2}}$, $\tilde{E} = \frac{Eg^2}{U_{10N}^4}$, where X is the fetch in m, and g is the gravitational constant. The state of wave development was expressed by the inverse wave age ($\frac{U_{10N}}{C_p}$).

[42] The radar observations were compared with the *Donelan et al.* [1992] empirical fetch-limited growth curves (equations (7) and (8)), hereafter DGC. The curves were derived from a series of tower observations and were based on the differential growth of wave energy between stations.

$$\tilde{X} = 40946 \ln\left[\frac{1}{1 - 5.5414\tilde{E}^{1/3.2}}\right] - 226900\left[1 + 2.7707\tilde{E}^{1/3.2}\right]\tilde{E}^{1/3.2} \tag{7}$$

$$\tilde{X} = 40946 \ln\left[\frac{\frac{U_{10N}}{C_p}}{\frac{U_{10N}}{C_p} - 0.8302}\right] - 33992\left(\frac{U_{10N}}{C_p} + 0.4151\right) \cdot \left(\frac{C_p}{U_{10N}}\right)^2 \tag{8}$$

[43] The 95% confidence intervals for the mean $\tilde{E}$ and $\frac{U_{10N}}{C_p}$ were estimated by varying H_s, T_m and U_{10N} over their respective 95 % confidence ranges. Because the observed quantities enter in both axes in Figures 8 and 9 the upper and lower bounds are expressed in both dimensions. Although the error range of the nondimensional fetch was small relative to the other two terms.

[44] As a first approach to the analysis U_{10N} was used directly to scale the observed energy and fetch (not shown). The observed $\tilde{E}$ growth with $\tilde{X}$ during each of the two cases was initially well below the DGC with $\tilde{X}$ determined by the distance from the shoreline to the observation point. At large fetches ($\tilde{X} > 4000$) the observed $\tilde{E}$ was much closer to DGC however there was more energy than anticipated on YD 356 and less on YD 361.

[45] Most previous studies of fetch-limited wave growth have relied on the assumption that the surface current velocity was wind-driven and consequently only a few percent of the wind velocity. This is not necessarily true if there are large tidal or mean flows, which occur in many coastal regions. The study area is an example of a region in which mean flows generated by basin scale winds dominate over the local wind-driven currents. The near-surface flows in the Florida Straits can reach 2 m s^{-1} in the core of the Florida Current [*Mooers and Fiechter*, 2005]. For all but the most extreme wind velocities these surface currents are much larger than the wind-driven flow. In both case studies U_a^0 reached 8–10% of U_{10N}. Scaling the current by the observed group velocity ($\frac{U^0}{Cg}$) revealed that the current velocities were a significant fraction of C_g during both periods. The ratio ranged from 0.1 close to the shoreline to 0.25 offshore on YD 356 and was consistently greater than 0. 4 on YD 361 (Figure 7). Therefore a correction was made to the DGCs such that the wind velocity used in the nondimensional terms took the mean flow into account through the equivalent neutral version of equation (1).

[46] The current velocity correction did not significantly change the wave energy growth on YD 356, except to shift the observations to shorter $\tilde{X}$ and lower $\tilde{E}$ (Figure 8a). This is because the opposing current produces a larger relative wind velocity, which enters each nondimensional parameter in the denominator. The effect of the current on $\tilde{E}$ is more pronounced because the relative velocity is raised to the 4th power. On YD 361 the shift was larger than on YD 356 because U_a^0 was a larger fraction of the wind speed (Figure 7). Here the initial growth was better represented in the DGC with U_r, but the large fetch results were shifted to lower energies than predicted. The shape of the growth curve has a different character than the previous observations and the difference in $\tilde{E}$ is well outside the 95 % confidence range.

[47] During both case studies there was a distance close to the shoreline over which the waves did not grow appreciably (Figure 8). The small wave limit below which the WERA could not observe the waves was $H_s \sim 0.1$m which corresponds to $\tilde{E} \sim 5 \times 10^{-6}$ on YD 356 and $\tilde{E} \sim 10^{-5}$ on YD 361. In both cases the observed $\tilde{E}$ values were above this lower limit and were considerably below the predicted value of $\tilde{E}$ from the DGC. The initial fetch beyond which the waves began to grow was 12-km ($\tilde{X} = 1073$) on YD 356 and 7-km ($\tilde{X} = 924$) on YD 361 as determined by inspection of the dimensional energy growth (not shown). It is interesting to note that the distance to the outer shelf (10-km, 7-km) was close to the distance over which $\tilde{E}$ did not increase appreciably. Given that the water depths inshore of the shelf edge can be less than 5-m it is possible that depth-limited effects were important. However, atmospheric boundary layer perturbations as the air passes over the tall buildings along the Key Biscayne shoreline may have also played a role.

[48] The initial growth of the surface waves was clearly disrupted in these experiments, although the precise mechanism for this disturbance was not known. Because of the availability of dense sampling at many fetches, corrections for the region of impaired growth were readily made. Adjusting the reference point (zero fetch) for DGC to the distance offshore at which the waves began to grow caused the observed $\tilde{E}$ to be much closer to the DGC. The fetch correction did not change the long fetch results appreciably because the DGC asymptotes to the same $\tilde{E}$ at large $\tilde{X}$.

[49] The inverse wave age was also scaled by the relative wind velocity U_r from (1). $\frac{U_r}{C_p}$ decreased with fetch as predicted on YD 356 with the waves remaining above the point of full development defined experimentally by *Donelan et al.* [1992] to be near $\frac{U_{10N}}{C_p} = 0.83$ (Figure 9). The DGC for inverse wave age predicted a much younger wave field at all fetches, with the exception of the peak in the observations near $\tilde{X} = 2900$. Because of the difficultly in

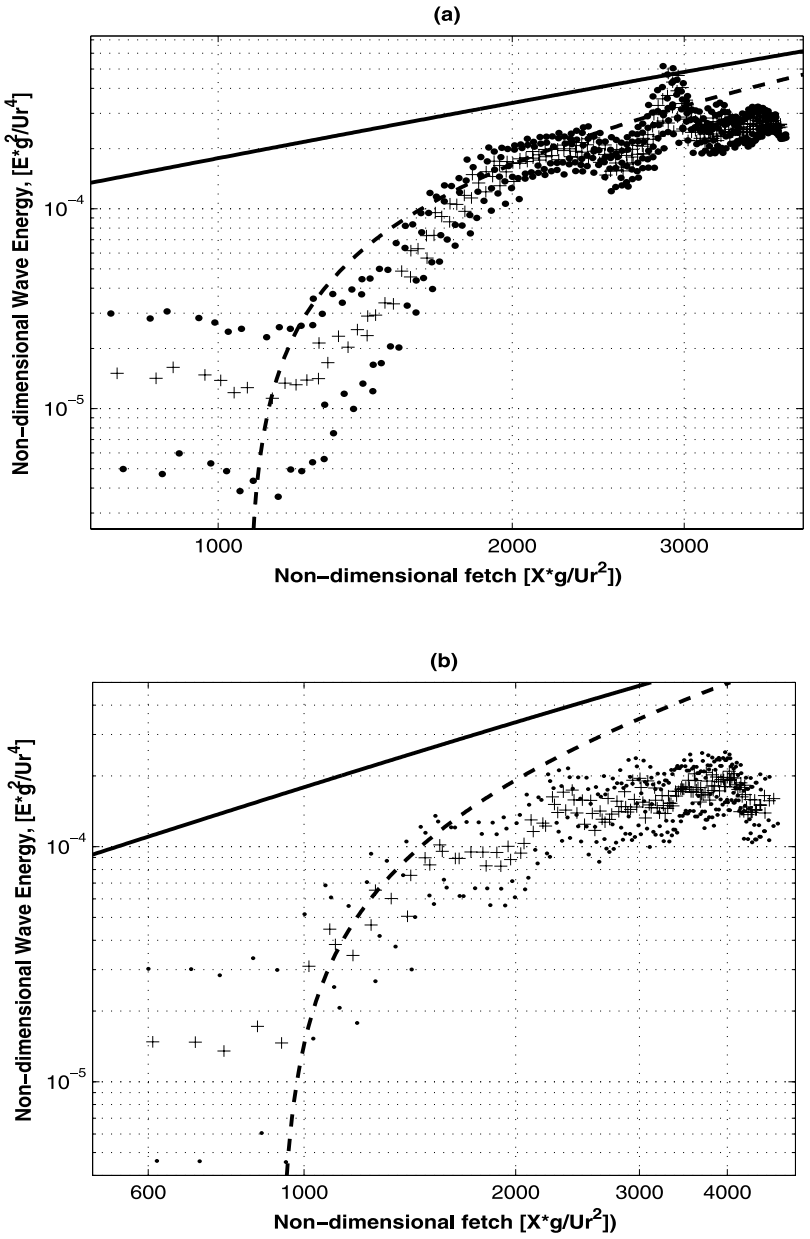

Figure 8. Nondimensional wave energy versus nondimensional fetch based on $U_r = (U_{10N} - U_a^0)$ included in nondimensional parameters. Pluses, mean energy growth. Dots, upper and lower 95% confidence intervals based on the variances of all observed terms. Solid line shows *Donelan et al.* [1992] curve as determined by the total fetch from the shoreline using $U_r = (U_{10N} - U_a^0)$. Dashed line shows result with U_r shifted to the point where the wave energy begins to grow as determined from zero intercept of SMB dimensional growth curve. (a) YD 356 (fetch shifted by 12 km). (b) YD 361 (fetch shifted by 7 km).

determining the initial point of wave growth it was instructive to look at the wave age decrease given an initial value of the DGC close to the observations. In this case the general trend of the observed decrease in $\frac{U_r}{C_p}$ with fetch was similar to the predictions.

[50] The shape of the observed growth curve was very different than the DGC, particularly for small $\tilde{X}$ on YD 356 and at large $\tilde{X}$ on YD 361. The wave growth was significantly less than predicted over the range from the point of initial growth until $\tilde{X} \sim 1800$. The difference between the DGC and the observations was well outside the 95% confidence interval over this range of fetches (Figure 8). This range of reduced growth could not be explained by depth-limitations as the shelf drops off sharply from the point of initial growth. Stability effects were also not likely to be important because as the waves moved offshore the water became warmer (Figure 6) and the interface remained unstable (Figure 5).

[51] *Drennan and Shay* [2006] have demonstrated that currents can cause the wind stress direction to shift in the direction of the current. This effect was shown to be significant in the absence of strong swell conditions, caus-

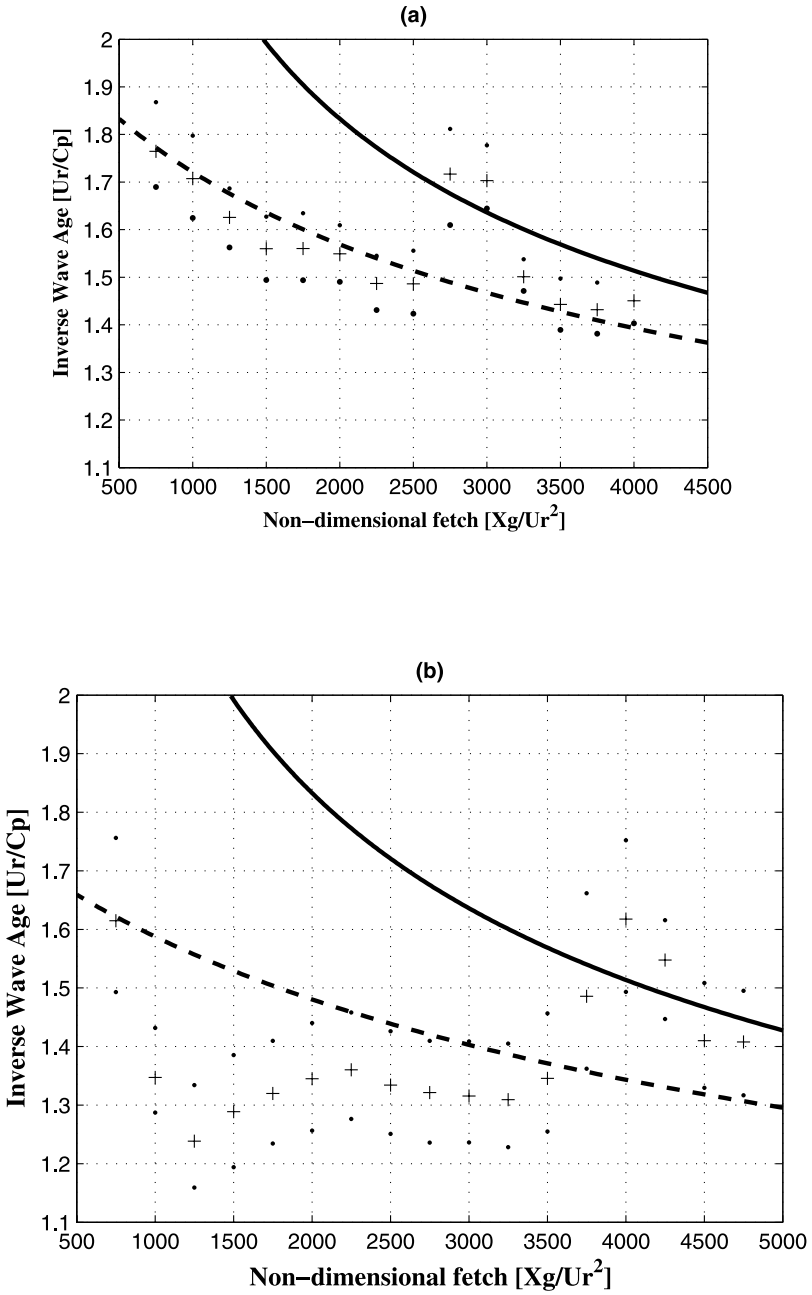

Figure 9. Inverse wave age (U_r/Cp) versus nondimensional fetch from WERA observations. Pluses, mean values over nondimensional fetch bins of 500; dots, 95% confidence intervals on estimate. Solid line is DGC based on total distance from shoreline. Dashed line is DGC shifted to match initial value. (a) YD 356 and (b) YD 361.

ing the off-wind stress angle to be as large as 45°. The mechanism for this wind-stress shift in the case of a sheared current was proposed to be the refraction of the dominant waves causing the short waves that support the wind stress to be shifted with the larger waves. Shifting the wind stress away from the wind direction would reduce the stress in the along-wind direction and suppress the wave growth rate.

[52] The amount of wave refraction over a sheared current will depend on the magnitude of ψ as determined by (4) [*Kenyon*, 1971] and in stronger currents the direction of wave propagation [*MacIver et al.*, 2006]. In these observations, ψ was continually varying and therefore the angle between the stress and the wind would change as well.

[53] The vertical component of vorticity (υ) defined in the wind-aligned coordinate system ranged from $-2.2\ f_c$ to $+1.3\ f_c$ (Figure 10). The suppression of the wave growth rate did not appear to depend on the sign of υ as the observed $\tilde{E}$ was below predicted for both positive and negative υ. This is consistent with refraction of the dominant surface waves away from their direction of propagation due to the current-shear. This would lead to less energy propagating in the wind direction as observed.

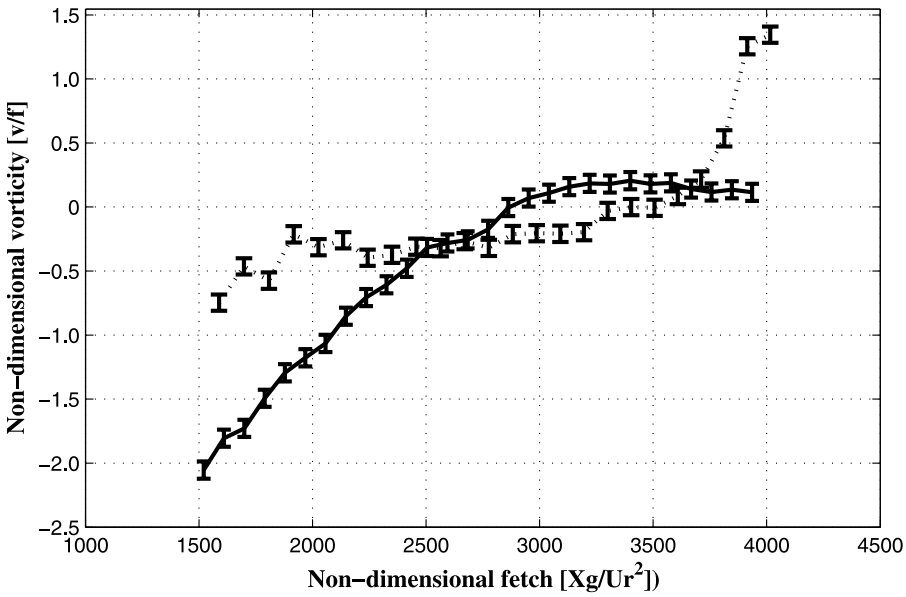

Figure 10. Vertical component of vorticity (υ) normalized by the local Coriolis parameter ($f_C = 6.28 \times 10^{-5}$ at 25.5° N) versus nondimensional fetch. YD 356 (solid line), YD 361 (dashed line). Error bars denote standard error of vorticity estimate.

[54] From the *Drennan and Shay* [2006] results maximum values of the veering of the wind stress direction reached 45°. Given that their observation were also made along the western edge of the FC, they are useful for estimating the scale of the effect observed here. This amount of directional deviation would cause a along-wind stress reduction of 30%. The predicted wave growth rate given this reduced stress would be 32% of the growth rate when the wind stress and wind were aligned.

[55] Taking the local slope of the observed $\tilde{E}$ vs. $\tilde{X}$ allowed the direct comparison of the energy growth rate with the DGC value. The observed wave energy growth rate in the high vorticity region between $1200 < \tilde{X} < 1500$ on YD 356 was only 29.5 % of the DGC rate. This reduction in growth rate was consistent with the expected rate if the wind stress deviated 45 % from the wind direction.

3.5. Trapping of Developing Waves in Opposing Currents

[56] There was a region of anomalously large energy located at $2.7 \times 10^3 < \tilde{X} < 3.0 \times 10^3$. The rate of increase of $\tilde{E}$ in this region (Figure 8) as well as the inverse wave age (Figure 9) were significantly (at the level of 95% confidence) larger than predicted by the DGC. $\tilde{E}$ was approximately doubled over the underlying trend. The higher energies were observed in the averaged values in 10 different cells, so this peak could not be attributed to a single outlier. After peaking at $\tilde{X} = 2.9 \times 10^3$ the dimensionless energy decayed rapidly to a level such that no net increase in growth was observed. During YD 361 some fluctuations about the general trend of increasing $\tilde{E}$ with $\tilde{X}$ occurred, but they were much reduced in amplitude relative to the YD 356 peak.

[57] The region of enhanced wave energy observed on YD 356 (Figure 8a) suggests that trapped waves are present in that area. The rapid decay with fetch supports this interpretation, because if the wave energy had been increased by momentum transfers from the wind then it should continue to propagate without significant decrease in energy. If the sheared current field is assumed to be a linear jet then wave ray theory predicts the formation of caustics at the maximum of the current when waves propagate obliquely into an opposing current [*Jonsson*, 1990], which is the situation in this case.

[58] *Kudryavtsev et al.* [1995] observed regions of enhanced wave energy in opposing currents within the core of the Gulf Stream. They demonstrated that if a curving jet is specified rather than a linear sheared current, then ray theory also allows trapping of waves in opposing currents. That the FC has local curvature in the study region can be clearly seen in the surface temperature images (Figure 6). From when the FC passes into the Florida Straits and then exits to the north it changes its flow direction from easterly to northerly with the peak of the curvature occurring in the region sampled on YD 356.

[59] On YD 361 there were fluctuations in the wave energy with fetch (Figure 8b) that were similar to the current normal laboratory observations of *MacIver et al.* [2006]. However, the amount of energy increase was much less than that observed on YD 356 and was not significant at the 95% confidence level. This was not surprising because the current was more normal to the wind direction (Figure 7) and in the swath sampled (Figure 3) the local curvature of the FC is typically less than along the shelf farther to the south.

[60] The Florida Current can be approximated as a linear or curved jet, in either case wave ray theory predicts that wave trapping can occur about the maximum of the current velocity. This point can be directly defined as the location where $\upsilon = 0$. The mean υ over both case study periods varied from -14×10^{-5} to 8.5×10^{-5} with fetch. Given the local Coriolis parameter of 6.28×10^{-5} this range encompasses Rossby numbers ($Ro = \upsilon/f_c$) from −2.2 on the

cyclonic (western) side of the FC to 1.3 on the anti-cyclonic (eastern) side of the FC (Figure 10). These values were roughly a factor of two larger than the horizontal shears observed by *Winkel et al.* [2002]. The sign of υ was opposite to their values because of the axes convention chosen for this study (Figure 3). It is likely that the larger R_o observed here was due to the denser horizontal sampling which allowed the high shear regions along the FC boundaries to be better resolved.

[61] On YD 356 a single zero-crossing of υ occurred at $\tilde{X}$ = 2900 (Figure 10), this exactly coincided with the region of sharply increased wave energy (Figure 8a). The wave energies then decreased to levels less than the trend predicted by the DGC as the vorticity increased. The waves also became much younger (Figure 9a) in the region where the wave energies increased. In both cases the local increases were well outside the 95% confidence intervals. These results confirm that the enhanced wave energies on YD 356 were due to trapping of waves about the vorticity zero-crossing, leading to energetic waves with short wavelengths.

[62] On YD 361 the vorticity trend was less clear, with small negative υ over the range from $\tilde{X}$ = 1900 to 3500. At the zero crossing point there was a slight increase (20%) in wave energy but this was within the 95 % confidence interval. There was sharply increased inverse wave age at longer fetches than the υ zero-crossing point as the seas became much younger (Figure 9b) due to the high positive υ. To determine the cause of the different response of the wave energy to the vorticity regime observed in the two case studies will require further study. Model comparisons and analysis of additional data sets should shed some light on the combination of wind velocity and vorticity likely to trap wave energy.

4. Conclusion

[63] The combination of WERA wave measurements during two periods of relatively steady offshore winds with the local near-surface current vector observations from the HF radar revealed several interesting features.

[64] The high spatial resolution of measurements in the wind direction enabled identification of the fetch at which the waves began to grow appreciably. This then provided a basis for elimination of the effects of the boundary layer transition region for the wave growth studies and would also allow a direct treatment of shallow water effects on wave growth.

[65] Because the alongwind current velocity was an order of magnitude larger than the wind driven component, it had a significant impact on the fetch-limited wave growth. This was anticipated because when one considers the standard [*Kitaigorodskii*, 1962] nondimensional parameters for fetch and energy the wind velocity enters each parameter as a power of 2 and 4, respectively. Adjusting the parameters to include the relative wind that has been shifted by the current can change the shape of the observed growth appreciably.

[66] Along the Florida Current western wall, the high local vorticity can cause significant suppression of developing waves. This suppression occurred even when the waves were moving into the current direction and increased wave energy would be expected because of the larger relative wind velocity and local wavenumber. The reduction in wave growth rates was consistent with a shift of the wind stress away from the wind direction, thereby reducing the momentum transfer to the waves. The wind stress shift was likely caused by the refraction of the dominant waves causing the short waves that support most of the stress but are riding along the larger waves to be shifted as well.

[67] A region of increased wave energy consistent with trapping caused by a sheared curving jet was directly observed. The local wave energy doubled at the point where the vertical vorticity was zero during one of the case studies. These regions of trapped waves could be areas in which hazards to marine operations are increased and may be a locus for the formation of very large (rogue) waves.

[68] A potential application for the near-real time current fields available from HF radars deployed in coastal observatories is to identify the locations where the vorticity changes sign. These locations where it is likely that wave energy will be trapped and create dangerous wave conditions could be provided to ships operating in the area. Where radar wave information is available as in the case of this study, the accuracy of these warnings could be directly assessed. This would be particularly relevant in strong current regimes such as the Gulf Stream, Kuroshio and the Agulhas current, all of which have been known to be regions where rogue waves have posed a hazard.

[69] **Acknowledgments.** I would like to thank the following people who have helped us with locations for the radars: Renate Skinner, Jim Duquesnel, and Eric Kiefer from Florida DEP for our site in North Key Largo Botanical Reserve. Kevin Kirwan and Ernest Lynk from Miami-Dade County Parks and Recreation for the site in Crandon Park on Key Biscayne. Thomas Cook and Jorge Martinez-Pedraja were critical to the research through their work with the WERA measurement group at the University of Miami. Frank Muller-Karger and Chuanmin Hu of the Institute for Marine Remote Sensing (IMaRS) at the College of Marine Science, University of South Florida, provided satellite imagery. I greatly appreciate the comments of Nick Shay, William Drennan and Mark Donelan on an early draft of this manuscript. This work was supported by the United States Office of Naval Research through the SEACOOS program.

References

Barrick, D. E. (1977), Extraction of wave parameters from measured HF radar sea-echo Doppler spectra, *Radio Sci.*, *12*(3), 415–424.

Beal, R., V. Kudryavtsev, D. Thompson, S. Grodsky, D. Tilley, V. Dulov, and H. Graber (1997), The influence of the marine atmospheric boundary layer on ERS-1 synthetic aperature radar imagery of the Gulf Stream, *J. Geophys. Res.*, *102*(C3), 5799–5814.

CERC (1977), Shore Protection Manual, 3 vols., U.S. Army Coastal Eng. Res. Cent., Washington, D. C.

Cornillion, P., and K.-A. Park (2001), Warm core ring velocities inferred from NSCAT, *Geophys. Res. Lett.*, *28*(4), 575–578.

Crombie, D. D. (1955), Doppler spectrum of sea echo at 13.56 $Mc.s^{-1}$, *Nature*, *175*, 681–682.

Dobson, F., W. Perrie, and B. Toulany (1989), On the deep-water fetch laws for wind-generated surface gravity waves, *Atmos. Ocean*, *27*, 210–236.

Donelan, M. A. (1990), Air-Sea Interaction, in *The Sea: Ocean Engineering Science*, vol. 9B, edited by B. LeMéhauté and D. Hanes, pp. 239–292, John Wiley, Hoboken, N. J.

Donelan, M. A., M. Skafel, H. Graber, P. Liu, D. Schwab, and S. Venkatesh (1992), On the Growth Rate of Wind-Generated Waves, *Atmos. Ocean*, *30*(3), 457–478.

Drennan, W. M., and L. K. Shay (2006), On the variability of the fluxes of momentum and sensible heat, *Boundary Layer Meteorol.*, *119*, 81–107, doi 10.1007/s10546-005-9010-z.

Essen, H. H., K. W. Gurgel, and T. Schick (2000), On the accuracy of current measurements by means of HF radar, *IEEE J. Oceanic Eng.*, *25*(4), 472–480.

Fiechter, J., K. L. Steffen, C. N. K. Mooers, and B. K. Haus (2006), Hydrodynamics and sediment transport in a South Florida tidal inlet,

Estuarine Coastal Shelf Sci., *70*, 297–306, doi:10.1016/j.ecss.2006.06.21.

Geernaert, G. L. (1988), Measurements of the angle between the wind vector and the wind stress vector in the surface layer over the North Sea, *J. Geophys. Res.*, *93*(C7), 8215–8220.

Geernaert, G. L., F. Hansen, M. Courtney, and T. Herbers (1993), Directional attributes of the ocean surface wind stress vector, *J. Geophys. Res.*, *98*, 16,571–16,582.

Graber, H. C., and M. L. Heron (1997), Wave height measurements from HF radar, *Oceanography*, *10*(2), 90–92.

Graber, H. C., B. K. Haus, L. K. Shay, and R. D. Chapman (1997), HF radar comparisons with moored estimates of current speed and direction: Expected differences and implications, *J. Geophys. Res.*, *102*, 18,749–18,766.

Graber, H. C., E. A. Terray, M. A. Donelan, W. M. Drennan, J. C. Van Leer, and D. B. Peters (2000), ASIS-a new air-sea interaction spar buoy: Design and performance at sea, *J. Atmos. Oceanic Technol.*, *17*(5), 708–720.

Grachev, A. A., C. W. Fairall, J. E. Hare, J. B. Edson, and S. D. Miller (2003), Wind stress vector over ocean waves, *J. Phys. Oceanogr.*, *33*, 2048–2429.

Gurgel, K.-W., G. Antonischki, H.-H. Essen, and T. Schlick (1999), Wellen Radar (WERA): A new ground-wave HF radar for ocean remote sensing, *Coastal Eng.*, *37*, 219–234.

Hasselmann, K., et al. (1973), Measurements of wind-wave growth and swell decay during the Joint North Sea Wave Project (JONSWAP), *Dtsch. Hydrogr. Z.*, *12*, suppl. A, 95 pp.

Haus, B. K., J. D. Wang, J. Rivera, N. Smith, and J. Martinez-Pedraja (2000), Remote radar measurement of shelf currents off Key Largo, Florida, *Estuarine Coastal Shelf Sci.*, *51*, 553–569.

Haus, B. K., J. D. Wang, J. Martinez-Pedraja, and N. Smith (2004), Southeast Florida shelf circulation and volume exchange: Observations of km-scale variability, *Estuarine Coastal Shelf Sci.*, *59*(2), 277–294.

Haus, B. K., R. Ramos, H. C. Graber, L. K. Shay, and Z. R. Hallock (2006), Remote observation of the spatial variability of surface waves interacting with an estuarine outflow, *IEEE J. Oceanic Eng.*, *31*(4), 835–849.

Heron, M. L., P. E. Dexter, and B. T. McGann (1985), Parameters of the air-sea interface by high-frequency ground-wave Doppler radar, *Aust. J. Mar. Freshw. Res.*, *36*, 655–670.

Hisaki, Y. (2005), Ocean wave directional spectra estimation from an HF ocean radar with a single antenna array: Observation, *J. Geophys. Res.*, *110*, C11004, doi:10.1029/2005JC002881.

Howell, R., and J. Walsh (1993), Measurement of ocean wave spectra using narrow-beam HF Radar, *J. Oceanic Eng.*, *18*, 296–305.

Hwang, P. A. (2006), Duration- and fetch-limited growth functions of wind-generated waves parameterized with three different scaling wind velocities, *J. Geophys. Res.*, *111*, C02005, doi:10.1029/2005JC003180.

Jonsson, I. G. (1990), Wave-current interaction, in *The Sea: Ocean Engineering Science*, vol. 9B, edited by B. LeMéhauté and D. Hanes, pp. 65–120, John Wiley, Hoboken, N. J.

Kenyon, K. (1971), Wave refraction in ocean currents, *Deep Sea Res.*, *18*, 1023–1034.

Kitaigorodskii, S. A. (1962), Applications of the theory of similarity to the analysis of wind-generated wave motion as a stochastic process, *Bull. Acad. Sci. USSR, Geophys. Ser.*, *1*, 105–117.

Kudryavtsev, V. N., S. A. Grodsky, V. A. Dulov, and A. N. Bol'shakov (1995), Observations of wind waves in the Gulf Stream frontal zone, *J. Geophys. Res.*, *100*(C10), 20,715–20,727.

MacIver, R. D., R. R. Simons, and G. P. Thomas (2006), Gravity waves interacting with a narrow jet-like current, *J. Geophys. Res.*, *111*, C03009, doi:10.1029/2005JC003030.

Mei, C. C. (1989), *The Applied Dynamics of Ocean Surface Waves*, World Sci., Hackensack, N. J.

Mooers, C. N. K., and J. Fiechter (2005), Numerical simulations of mesoscale variability in the Straits of Florida, *Ocean Dyn.*, *55*, 309–325, doi:10.1007/s10236-005-0019-0.

Ramos, R. J. (2006), 2-D analysis of wave energy evolution using wavelet transforms, Ph.D. thesis, Univ. of Miami, Miami, Fla., March.

Rieder, K. F., J. A. Smith, and R. A. Weller (1994), Observed directional characteristics of the wind, wind stress and surface waves on the open ocean, *J. Geophys. Res.*, *99*(C11), 22,589–22,596.

Shay, L. K., P. C. Zhang, H. C. Graber, and E. J. Walsh (1996), Simulated surface wave current interactions during SWADE, *Global Atmos. Ocean Syst.*, *5*, 125–150.

Shay, L. K., et al. (2000), VHF radar detects oceanic submesoscale vortex along Florida coast, *Eos Trans. AGU*, *81*, 209,213.

Shay, L. K., J. Martinez-Pedraja, T. M. Cook, B. K. Haus, and R. H. Weisberg (2007), High-frequency radar mapping of surface currents using WERA, *J. Atmos. Oceanic Technol.*, *24*(3), 484–503.

Walsh, E. J., L. K. Shay, H. C. Graber, A. Guillaume, D. Vandemark, D. E. Hines, R. N. Swift, and J. F. Scott (1996), Observations of surface wave-current interaction during SWADE, *Global Atmos. Ocean Syst.*, *5*, 99–124.

Winkel, D. P., M. C. Gregg, and T. B. Sanford (2002), Patterns of shear and turbulence across the Florida Current, *J. Phys. Oceanogr.*, *32*, 3269–3285.

Wyatt, L. R. (1990), A relaxation method for integral inversion applied to HF radar measurement of the ocean wave directional spectrum, *Int. J. Remote Sens..*, *11*, 1481–1494.

Wyatt, L. R., S. P. Thompson, and R. R. Burton (1999), Evaluation of high frequency radar wave measurement, *Coastal Eng.*, *37*, 259–282.

Wyatt, L. R., G. Liakhovetski, H. Graber, and B. K. Haus (2005), Factors affecting the accuracy of Showex HF radar wave measurements, *J. Atmos. Oceanic Technol.*, *22*, 847–859.

Young, I. R. (1997), The growth rate of finite depth wind-generated waves, *Coastal Eng.*, *32*, 181–195.

Zemba, J., and C. A. Friehe (1987), The marine atmospheric boundary layer jet in the Coastal Ocean Dynamics Experiment, *J. Geophys. Res.*, *92*, 1289–1496.

B. K. Haus, Division of Applied Marine Physics, Rosenstiel School of Marine and Atmospheric Science, University of Miami, Miami, FL 33149-1098, USA. (bhaus@rsmas.miami.edu)